DEMIS: Electron Microscopy Image Stitching Using Deep Learning Features and Global Optimisation

Petr Šilling[a] and Michal Španěl[b]

Department of Computer Graphics and Multimedia, Brno University of Technology, Brno, Czech Republic

fi fi

Keywords: Electron Microscopy, Whole Slide Imaging, Image Stitching, Neural Networks.

Abstract: Accurate stitching of overlapping image tiles is essential for reconstructing large-scale Electron Microscopy (EM) images during Whole Slide Imaging. Current stitching approaches rely on handcrafted features and translation-only global alignment based on Minimum Spanning Tree (MST) construction. This results in sub-optimal global alignment since it neglects rotational errors and works only with transformations estimated from pairwise feature matches, discarding valuable information tied to individual features. Moreover, handcrafted features may have trouble with repetitive textures. Motivated by the limitations of current methods and recent advancements in deep learning, we propose DEMIS, a novel EM image stitching method. DEMIS uses Local Feature TRansformer (LoFTR) for image matching, and optimises translational and rotational parameters directly at the level of individual features. For evaluation and training, we create EM424, a synthetic dataset generated by splitting high-resolution EM images into arrays of overlapping image tiles. Furthermore, to enable evaluation on unannotated real-world data, we design a no-reference stitching quality metric based on optical flow. Experiments that use the new metric show that DEMIS can improve the average results from 32.11 to 2.28 compared to current stitching techniques (a 1408% improvement). Code is available at: https://github.com/PSilling/demis.

1 INTRODUCTION

Whole Slide Imaging is a technique for capturing large biological samples that do not fit under the field of view of a single electron microscope. To accomplish this, the sample is scanned in sections, creating an array of tiles with a set overlap. The tiles are then stitched into a composite image with a wide view and higher resolution. To produce a high quality composite image, an accurate image stitching algorithm is essential. However, there are multiple challenges in electron microscopy image stitching that may not appear in other applications: (a) the presence of repetitive texture patterns, which may degrade image registration results, (b) the occurrence of empty areas with low quality texture and few informative features, and (c) the extensive size of the stitched arrays (commonly containing tens or even hundreds of ultra high-definition images), which requires the use of algorithms that can mitigate the gradual accumulation of stitching errors.

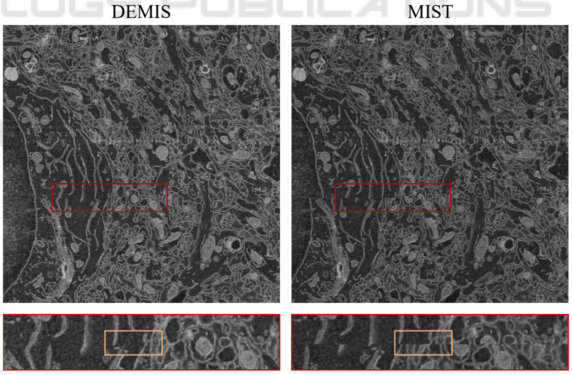

Figure 1: Stitching comparison of DEMIS and MIST (Chalfoun et al., 2017) on real-world data. MIST produces significantly more misalignments than DEMIS.

Current microscopy stitching methods split tile stitching into two steps: (1) pairwise registration, which estimates transformations between adjacent tiles, and (2) global alignment, which minimises error propagation in the final composite image (Chalfoun et al., 2017; Muhlich et al., 2022; Mahalingam et al., 2022; Mohammadi et al., 2024b; Shi et al., 2024). For pairwise registration, current approaches

[a] https://orcid.org/0000-0001-5921-8109
[b] https://orcid.org/0000-0003-0193-684X

Šilling, P. and Španěl, M.
DEMIS: Electron Microscopy Image Stitching Using Deep Learning Features and Global Optimisation.
DOI: 10.5220/0013314900003911

In *Proceedings of the 18th International Joint Conference on Biomedical Engineering Systems and Technologies (BIOSTEC 2025) - Volume 1*, pages 255-265
ISBN: 978-989-758-731-3; ISSN: 2184-4305

rely on traditional image registration techniques, such as Normalised Cross-Correlation (Lewis, 1995) or SIFT (Lowe, 2004). While these techniques produce satisfactory results on most images, they may struggle with highly repetitive or exceedingly low-quality textures, which may lead to alignment errors. Moreover, current methods assume the movement of the mechanical stage is precise enough to generate translational shifts only. Consequently, they limit the estimated transformation parameters to translation. Since other misalignments, such as slight rotational shifts, might be present in some samples, the alignment errors might be increased further. The intensity of these errors should be minimised by the subsequent global alignment stage. However, most current approaches employ a Minimum Spanning Tree (MST) algorithm or a comparable technique to select the set of pairwise transformations that minimise the global error. Doing so does not directly optimise the pairwise transformations. As a result, the quality of the final image remains limited by the accuracy of pairwise transformations. Figure 1 highlights the alignment errors produced by current methods on challenging input where translation-only transformation estimation is not sufficient.

Motivated by the above issues, we propose Deep Electron Microscopy Image Stitching (DEMIS), a novel approach to stitching electron microscopy images. Inspired by the recent advancements in feature detection and matching using deep neural networks (DeTone et al., 2018; Sarlin et al., 2020), we suggest to use Local Feature TRansformer – LoFTR (Sun et al., 2021) to detect feature matches in the pairwise registration stage. Additionally, we propose to estimate both translational and rotational transformation parameters from the detected matches. DEMIS does so by formulating a non-linear least squares optimisation problem, which estimates global tile poses (positions and rotations) by minimising the total feature reprojection error. Since DEMIS optimises feature matches directly without first evaluating transformations between adjacent tiles, it avoids the limitations of MST-based optimisation. The global poses are used to create the final composite image.

To evaluate DEMIS and train LoFTR, we additionally propose EM424, a novel synthetic dataset created from 424 public electron microcopy images with high resolution. The dataset is generated by randomly splitting the microscopy images into arrays of overlapping image tiles and by applying random noise and intensity changes. The dataset is available as a part of this work. Furthermore, inspired by Electron Microscopy Stitched Image Quality Assessment – EMSIQA (Shi et al., 2024), we propose Optical Flow Stitched Image Quality Assessment (OFSIQA), a no-reference stitching evaluation metric based on the magnitude of optical flow in the overlapping regions of adjacent image tiles.

We evaluate DEMIS and OFSIQA on the synthetic dataset and we use OFSIQA to further evaluate DEMIS on a challenging real-world biological dataset provided by the company TESCAN 3DIM[1]. The experiments show that DEMIS outperforms the current state-of-the-art solutions, such as Microscopy Image Stitching Tool – MIST (Chalfoun et al., 2017), on both feature matching accuracy and final image output quality on multiple quality assessment metrics. The experiments also demonstrate a positive impact of rotational parameter estimation on stitching accuracy.

To summarise, the main contributions of this paper are as follows:

- We introduce DEMIS, a novel electron microscopy image stitching method based on LoFTR and least squares global optimisation of translational and rotational transformation parameters. We show that DEMIS outperforms current state-of-the-art solutions, especially on real-world data.
- We prepare EM424, a novel synthetic image stitching dataset generated from 424 publicly available high-quality electron microscopy images. Compared to current microscopy datasets, EM424 includes reference transformations, which enable precise stitching evaluation.
- We propose OFSIQA, a no-reference image stitching quality assessment metric based on the magnitude of optical flow. We estimate the optical flow using the RAFT network (Teed and Deng, 2020).

2 RELATED WORK

Image Registration and Matching. Traditionally, image registration methods can be divided into intensity-based and feature-based approaches. Intensity-based methods, most notably Normalised Cross-Correlation (Lewis, 1995) and Phase Correlation (Kuglin and Hines, 1975), work by finding correlations in intensity between the registered images. Feature-based registration methods detect sparse sets of features in each registered image. The features are then matched and used to estimate registration parameters. The first widely adopted feature descriptor was

[1] https://www.tescan3dim.com/

SIFT (Lowe, 2004). Other feature descriptors, such as SURF (Bay et al., 2006), ORB (Rublee et al., 2011), and KAZE (Alcantarilla et al., 2012), tried to enhance the speed or accuracy of SIFT. Despite that, SIFT arguably remained the golden standard for feature detection in terms of accuracy.

Recently, deep learning approaches have started to improve on the traditional techniques. The pioneering work in this area is SuperPoint (DeTone et al., 2018), which presents a fully convolutional feature extraction network that outperforms conventional techniques, especially on noisy images and under large illumination changes. SuperPoint is further improved by SuperGlue (Sarlin et al., 2020), which uses a graph neural network to find correspondences between the detected features. The concepts from SuperPoint and SuperGlue are then effectively combined to form LoFTR (Sun et al., 2021), an attention-based feature detection and matching network. LoFTR further improves feature matching performance, especially on areas with less texture or repetitive patterns. Current works focus on improving LoFTR. In particular, ASpanFormer (Chen et al., 2022) introduces attention spans with sizes that adapt to global and local context characteristics. MatchFormer (Wang et al., 2023) better leverages the encoder using a novel hierarchical architecture with interleaving self-attention and cross-attention. Finally, AdaMatcher (Huang et al., 2023) addresses the inconsistencies caused by the mutual nearest neighbour matching criterion.

Microscopy Image Stitching. One of the first tools for stitching electron microscopy images was TrakEM2 (Cardona et al., 2012), an ImageJ (Schneider et al., 2012) plugin that features a SIFT-based image stitching algorithm. A more recent tool, MIST (Chalfoun et al., 2017), employed Normalised Cross-Correlation to compute image registrations. Additionally, MIST estimated the parameters of the mechanical stage and constructed a Minimum Spanning Tree (MST) to minimise global errors. By doing so, MIST achieved state-of-the-art performance. Li and Ding then proposed a stitching technique based on SURF features and PCA dimensionality reduction (Li and Ding, 2018; Jolliffe, 2002). Evaluation on ceramic microscopy images displayed slightly better performance than traditional SIFT-based stitching. Mahalingam et al. introduced a highly-scalable pipeline for stitching microscopy datasets composed of up to petabytes of data (Mahalingam et al., 2022). The pipeline uses SIFT feature detection aided by lens distortion estimation. Furthermore, Muhlich et al. presented a registration method for multiplexed images based on Phase Correlation and MST construction (Muhlich et al., 2022). Zhao et al. proposed a smoothing strategy that gradually transforms general perspective transformations applied to overlapping regions of stitched tiles to linear-only transformations applied to non-overlapping areas (Zhao et al., 2023). Fast and Robust Microscopic Image Stitching – FRMIS (Mohammadi et al., 2024b) then improved the speed of tile registration by primarily detecting SURF features in only small segments of the overlapping regions. Finally, a two-stage error-correcting pipeline was introduced, which showed accuracy comparable to other feature-based approaches at a significant increase in speed (Shi et al., 2024). Deep learning approaches to microscopy image stitching remain largely unexplored, with only a recent study (Mohammadi et al., 2024a) evaluating SuperPoint features and reporting mixed results.

Microscopy Image Stitching Datasets. In electron microscopy, stitching can generally be considered a preprocessing step that is necessary for further data analysis and biological research. The majority of public microscopy datasets, such as the MICrONS mouse visual cortex dataset (The MICrONS Consortium et al., 2021), are therefore composed of already stitched images or are tailored to other image processing tasks, such as image segmentation (Conrad and Narayan, 2021). A single stitching-related dataset was created for the evaluation of MIST (Chalfoun et al., 2017). The dataset includes scans of stem colonies at various stages of growth and with known colony centroid positions. The centroid positions can then be used to measure stitching error. However, the centroid errors cannot evaluate the quality of individual transformations. Furthermore, the dataset is rather domain-specific and contains only simple translational shifts. In this paper, we introduce EM424, a novel synthetic dataset that addresses these shortcomings.

Microscopy Stitching Quality Assessment. Microscopy image stitching datasets are generally private and without ground-truth annotations. Consequently, the use of conventional reference-based image quality assessment metrics, such as PSNR and SSIM (Zhou et al., 2004), is challenging. As a result, the quality of stitched microscopy images is commonly measured by (a) a qualitative analysis of the final output and stitching errors, (b) feature detection statistics, such as total feature and outlier counts, or (c) no-reference image quality metrics. Shi et al. recently introduced EMSIQA, a no-reference stitching quality metric designed specifically for microscopy

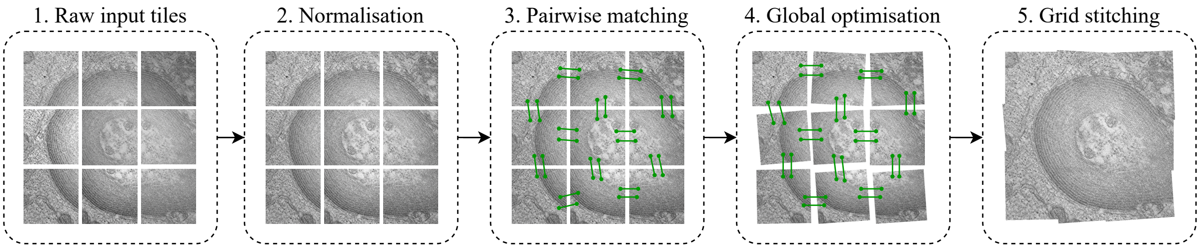

Figure 2: Overview of the stitching pipeline used by DEMIS. First, the brightness and contrast of raw input images are normalised. Second, for each pair of adjacent images, features are detected and matched by LoFTR (Sun et al., 2021). Subsequently, a least squares model of the stitched grid is constructed based on the expected grid structure and the detected feature matches. In the model, each image is represented by its pose and related to adjacent images by the corresponding matches. The modelled poses are optimised globally using the Levenberg-Marquardt algorithm (Marquardt, 1963). Finally, the grid is stitched by gradually drawing individual image tiles transformed according to the optimised poses. The image tiles were acquired from a scan of cytoplasmic multilamellar structures (Beyer et al., 2009).

images (Shi et al., 2024). EMSIQA is designed around optical flow weighted by binary masks produced by OTSU thresholding (Otsu, 1979). In this paper, we propose OFSIQA, a modified version of EMSIQA, which we use for evaluation on data with no reference transformations.

3 PROPOSED STITCHING METHOD

We introduce the proposed method in three steps. First, we present a pairwise feature matching approach for grids of overlapping image tiles based on LoFTR. Second, we formulate a least squares optimisation problem to obtain globally optimal tile transformations from pairwise feature matches. Finally, we define OFSIQA using optical flow measurements. The first two steps form the foundation of DEMIS and are outlined in Figure 2.

3.1 Pairwise Feature Matching

Let G be the grid of overlapping electron microscopy images with an expected overlap ratio $o \in (0,1)$. We find feature matches between all pairs of adjacent tiles in G in the following way.

First, the raw image tiles are normalised to ensure that any brightness and contrast inconsistencies caused by the sequential nature of Whole Slide Imaging do not negatively affect feature detection and matching or the visual aspects of the final stitched image. Contrast-Limited Adaptive Histogram Equalisation (Pizer et al., 1987) is used to perform the normalisation. An adaptive normalisation method is necessary since the content in different parts of electron microscopy images can vary considerably.

Subsequently, for all pairs of adjacent tiles (I_1, I_2) in G, I_1 and I_2 are cropped by the overlap ratio o, producing cropped images I_1' and I_2'. I_1' and I_2' contain the expected overlapping regions of I_1 and I_2, respectively. The direction from which to crop can be determined from the relative positions of both images. The cropping significantly reduces the amounts of computation time and memory required for feature matching.

Finally, LoFTR is used to detect and match features between all pairs of cropped images I_1' and I_2'. The positions of the matches are corrected to fit the original images I_1 and I_2 by reversing the cropping operation. We assume the tiles have a sufficiently large overlap for LoFTR to produce a valid result. From our empirical observations, a 10% overlap is generally acceptable. However, the specific requirement depends considerably on the quality and resolution of the processed images.

In traditional stitching pipelines, the detected matches are most commonly used to directly estimate the transformation matrix that relates I_1 to I_2, e.g., using Random Sample Consensus – RANSAC (Fischler and Bolles, 1981). The transformation estimates from all image pairs could then be optimised globally. However, doing so could discard potentially valuable information tied to individual feature matches. Therefore, we propose to run the optimisation on the level of features instead of transformations, as described in detail in the following section.

3.2 Global Optimisation and Alignment

To avoid the limitations of transformation-based optimisation, we solve global alignment by formulating a non-linear least squares optimisation problem at the level of individual feature matches. We build a model where each image tile in G is represented by its pose, i.e., its position and rotation angle. The initial position estimates are set based on tile resolution and the

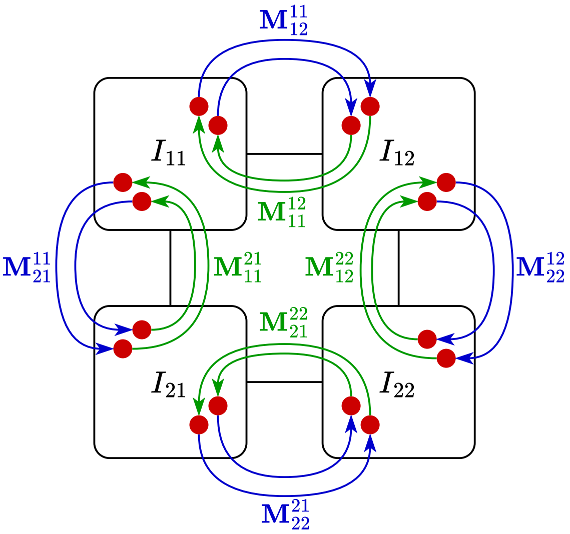

Figure 3: Graphical representation of the proposed global optimisation model on a sample 2×2 image grid. Each image in the model is represented by three pose parameters and is connected to adjacent images by the corresponding feature matches.

expected overlap o. In particular, for tile I_{rc} at a row-major grid index (r,c), its initial position parameters p_{rc}^{x} and p_{rc}^{y} are calculated as

$$\begin{aligned} p_{rc}^{x} &= (1-o)\cdot w\cdot (c-1), \\ p_{rc}^{y} &= (1-o)\cdot h\cdot (r-1), \end{aligned} \tag{1}$$

where w and h are the width and height of the images in G. The initial angles α_{rc} are set to zero. In other words, the initial poses correspond to the ideal case scenario, in which no misalignments between tiles exist and the expected overlaps are correct.

Let us denote the column matrix of features matched from a source image I_{rc} to a target image I_{ij} in homogenous coordinates as $\mathbf{M}_{ij}^{rc}$. We minimise the total feature reprojection error, i.e., the distance between matched features after projection to the global coordinate space. To do so, we first transform all matched features according to the current pose parameters of their source image tile. For $\mathbf{M}_{ij}^{rc}$, this yields its transformed matrix $\hat{\mathbf{M}}_{ij}^{rc}$ as

$$\hat{\mathbf{M}}_{ij}^{rc} = \begin{bmatrix} \cos\alpha_{rc} & -\sin\alpha_{rc} & p_{rc}^{x} \\ \sin\alpha_{rc} & \cos\alpha_{rc} & p_{rc}^{y} \\ 0 & 0 & 1 \end{bmatrix} \mathbf{M}_{ij}^{rc}. \tag{2}$$

We then measure the reprojection error E_{rep} as the sum of squared differences between $\hat{\mathbf{M}}_{ij}^{rc}$ and its opposite $\hat{\mathbf{M}}_{rc}^{ij}$ for all pairs of adjacent image tiles (I_{rc}, I_{ij}). Each of the differences is weighted by the corresponding match confidence score assigned by LoFTR. The relationship between image tiles and feature matrices is illustrated in Figure 3.

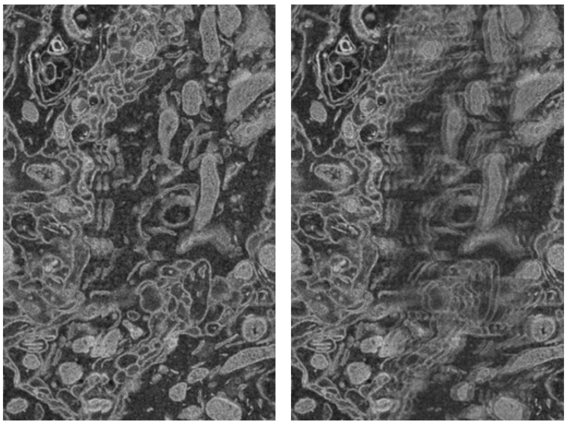

(a) Pixel replacement (b) Pixel averaging

Figure 4: Comparison of pixel replacement and pixel averaging on a stitched pair of image tiles with misalignment errors. Noticeable blurring can be seen when pixel averaging is used.

We optimise E_{rep} with respect to tile pose parameters using the Levenberg-Marquardt algorithm (Marquardt, 1963). During the optimisation, the parameters of the first tile, i.e., p_{11}^{x}, p_{11}^{y} and α_{11}, are locked to their initial values to ensure that the final stitched image has a predictable structure. The globally optimised parameters are then used to warp the corresponding image tiles in G, and the final composite image is constructed from the warped images. To avoid blurring in case of misalignments, any already filled pixels in the overlapping regions of multiple image tiles are simply replaced by the pixels of subsequently processed images without any form of pixel averaging. Figure 4 illustrates the difference in blurring between pixel replacement and pixel averaging.

3.3 Measuring Stitching Quality Using Optical Flow

We design the proposed OFSIQA metric as a modified version of EMSIQA (Shi et al., 2024), a recent no-reference stitching quality metric for biomedical electron microscopy images. We first introduce the fundamental concepts of EMSIQA, and then present our modifications.

Similarly to the pairwise matching algorithm, let I_1 and I_2 be two registered images and I_1' and I_2' their cropped overlapping regions. EMSIQA of I_1 and I_2 is then evaluated in three main steps. First, optical flow between I_1' and I_2' is estimated with FlowNet2 (Ilg et al., 2017). Afterwards, OTSU thresholding (Otsu, 1979) is applied to create binary segmentation masks of I_1' and I_2'. The segmentation masks are used to mask empty regions with no organelles in the predicted optical flow, accentuating organelle edges. Finally, EMSIQA is calculated as the average magnitude of the masked optical flow vectors normalised by the Dice coefficient (Dice, 1945) of the segmentation masks.

While the above process results in a functional stitching metric, it can be significantly simplified. EMSIQA attempts to use OTSU thresholding to focus its calculations more on edges and less on background noise. However, as shown in Figure 5, OTSU thresholding is unreliable for edge emphasis since it is not an edge nor a ridge detection method but a method for separating the foreground from the background. As such, it may fail to correctly highlight the biological structure in the images. Additionally, we observed that even masking noisy image regions using proper ridge detection techniques has little effect on metric quality since modern optical flow estimators are capable of robust motion interpolation.

Considering the above issue, we eliminate the OTSU thresholding steps and calculate the average magnitude of optical flow vectors directly from the initial optical flow. Formally, we define the OFSIQA of I_1 and I_2 as

$$\text{OFSIQA}(I_1, I_2) = \frac{1}{N} \sum_{(d_x,d_y)\in\mathcal{F}} \sqrt{d_x^2 + d_y^2}, \quad (3)$$

where N is the number of pixels in the overlapping region of I_1 and I_2 and $\mathcal{F}$ the set of all displacement vectors (d_x, d_y) in the optical flow between I_1' and I_2'.

Furthermore, we propose to estimate optical flow with RAFT (Teed and Deng, 2020) instead of FlowNet2. Doing so provides two primary benefits: (1) the architecture of RAFT is more robust and results in higher accuracy and efficiency, and (2) RAFT is easily accessible through torchvision[2], a widespread Python library for computer vision. We believe both performance and ease-of-use are essential for quality metrics and their adoption. Figure 6 depicts the calculation steps of OFSIQA.

4 DATASETS

EM424. Since the majority of public microscopy data is already in stitched form or contains no reference tile transformations, we prepare EM424, a synthetic dataset created from high-quality and high-resolution electron microscopy images publicly available on EMPIAR[3] or CIL[4]. A total of 424 individual images (259 from EMPIAR, 165 from CIL) from 36 different public projects were selected for the dataset. Each of the selected images has a resolution of at least 2048 × 2048 pixels and the majority of its area filled with a high-quality scan of the imaged sample instead of background noise. The selected images include scans of different kinds of human and animal tissue, proteins, bacteria and viruses.

The images were then split into as many overlapping image tiles of size 1024 × 1024 pixels as the original image resolution allowed. Each image tile was generated as follows. First, the base tile position was determined based on a uniformly selected overlap be-

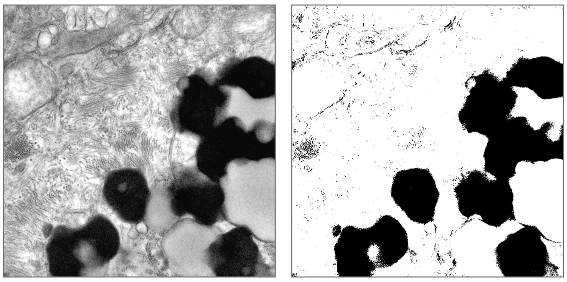

(a) Original image (b) OTSU thresholding

Figure 5: Example of inappropriate use of OTSU thresholding (Otsu, 1979) on an image of a human neocortex (Ellisman et al., 1987) during the calculation of EMSIQA (Shi et al., 2024). Since the input image has large contrast variance, the thresholded image fails to correctly highlight the biological structure in the majority of the image. As a result, EMSIQA would focus more on background noise, not the biological structure.

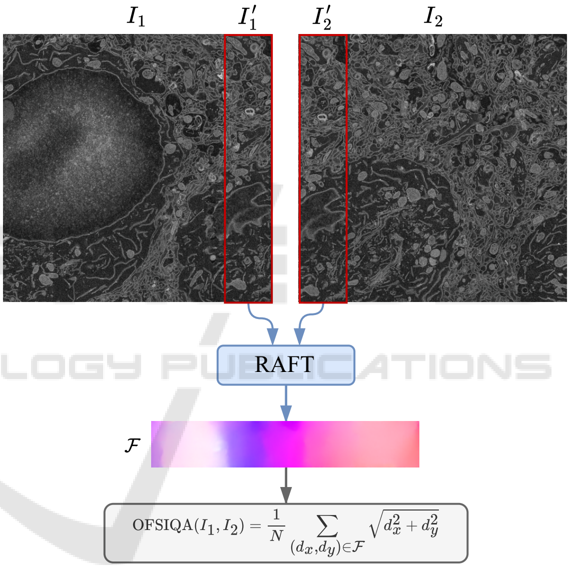
I_1
I_1'
I_2'
I_2
RAFT
$\mathcal{F}$
$\text{OFSIQA}(I_1, I_2) = \frac{1}{N} \sum_{(d_x,d_y)\in\mathcal{F}} \sqrt{d_x^2 + d_y^2}$

Figure 6: Computation of the proposed OFSIQA metric. The metric is calculated as the average magnitude of optical flow vectors in the overlapping region. The optical flow is estimated by RAFT (Teed and Deng, 2020).

[2] https://pytorch.org/vision/

[3] https://www.ebi.ac.uk/empiar/

[4] http://cellimagelibrary.org/

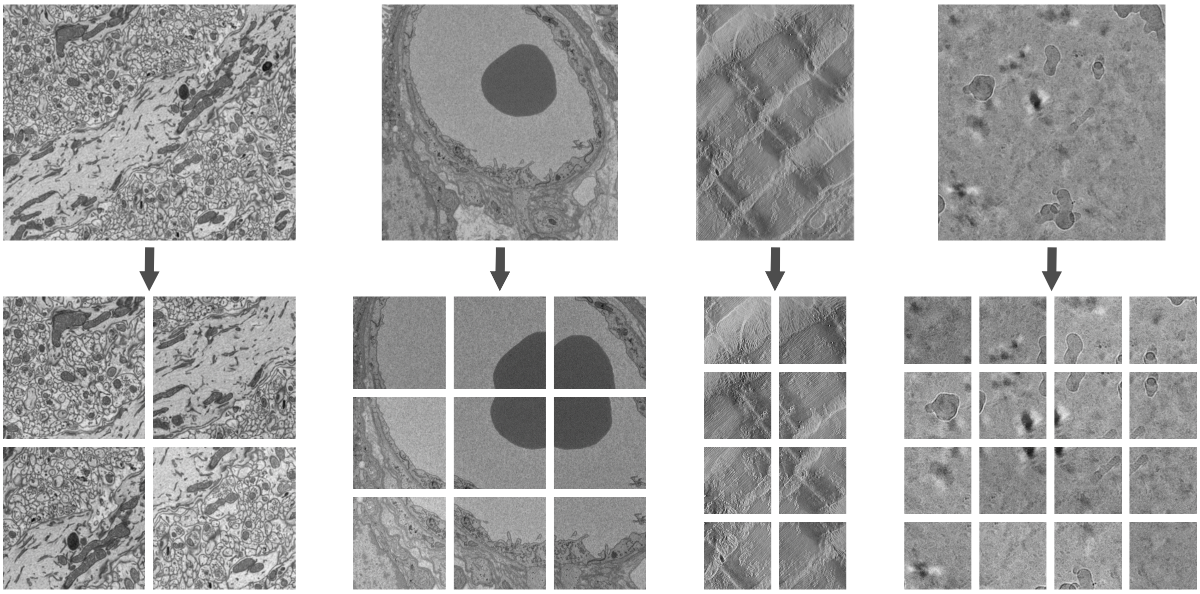

Figure 7: The splitting of image tiles for the EM424 dataset. The images are split into arrays of overlapping tiles 1024×1024 pixels in size. The number of generated tiles depends on the resolution of the source image. The displayed source images were retrieved from public microscopy datasets (Bushong and Deerinck, 2017; Lewis et al., 2022; Hoshijima et al., 2004; Liang et al., 2022).

tween 17% and 23% of the tile resolution. Second, the original image was rotated around the chosen tile position by up to 5 degrees in either direction using a uniformly selected random rotation angle. Then, the tile was cropped from the rotated source image at its calculated position. Finally, Gaussian noise and random brightness and contrast changes were applied to the tile to simulate scanning imperfections. Gaussian distributions with zero means and variances of 25, 75, and 0.0033, respectively, were used to generate the parameters of these augmentations.

In total, the above process resulted in 8339 image tiles separated into arrays of 4 to 162 images. 6282 of the tiles were selected for training, 751 for validation, and 1306 for evaluation. All tiles were labelled by ground-truth tile positions and rotation angles to enable reference reconstruction. The generation procedure and sample data are displayed in Figure 7.

Real-2x2. To demonstrate the viability of our solution in real-world applications, we supplement our synthetic dataset with Real-2x2, a dataset nominated by TESCAN 3DIM as challenging for current stitching algorithms. The dataset contains 2×2 scans of a single biological sample taken at 13 different slice positions (52 images in total). The tiles have a resolution of 4096×3072 pixels and an average 15% tile overlap. Figure 1 shows a sample taken from the Real-2x2 dataset.

5 IMPLEMENTATION DETAILS

We implemented DEMIS in Python using PyTorch, OpenCV, scikit-image and LMFIT. To limit any potential side effects of transformations found in conventional photography but not in electron microscopy, such as perspective deformations, we also fine-tuned the official outdoor weights of LoFTR on the training set of the EM424 dataset. The computational resources for fine-tuning were provided by e-INFRA CZ project (ID: 90140), supported by the Ministry of Education, Youth and Sports of the Czech Republic. We trained LoFTR for 8 epochs with the initial learning rate set to 1×10^{-5}. The code is available online under the MIT and Apache 2.0 licences.

6 EXPERIMENTS

To evaluate DEMIS, we compare its performance on various feature detection and stitching quality metrics against several baseline solutions. We conduct our experiments on the evaluation split of the EM424 dataset and on the Real-2x2 dataset. A machine with a 20-core, 5.60 GHz Intel Core i7-14700K CPU, an NVIDIA RTX 4090 GPU with 24 GB of memory, and 64 GB of RAM was used to run the experiments. The metrics and baseline solutions are introduced below.

Table 1: Stitching results on the synthetic EM424 dataset. DEMIS improves the results of conventional feature-based approaches in both feature quality and image quality metrics. Provided a system with a GPU is available, DEMIS does so at a reasonable cost to stitching time.

	Seconds	Matches	Reprojection error	RMSE	PSNR	SSIM	OFSIQA
SIFT	0.21 (CPU)	**1000**	2.86	20.73	21.97	0.69	1.21
ORB	**0.07 (CPU)**	289	4.18	20.70	21.98	0.69	1.22
DEMIS	0.27 (GPU)	**1000**	**2.83**	**20.41**	**22.10**	**0.70**	**1.19**

Feature Detection Metrics. For feature detection evaluation, we report the mean number of matches detected between adjacent tiles (limited to 1000 for performance reasons). On the EM424 dataset, we also report the mean feature reprojection error.

Image Stitching Metrics. For stitching evaluation, we measure the mean amount of time to stitch one tile in seconds and the mean RMSE, PSNR, SSIM (Zhou et al., 2004) and OFSIQA of the stitched images. For the Real-2x2 dataset, only time and OFSIQA are reported due to the absence of reference images.

Baseline Solutions. We compare DEMIS against four baseline solutions:

- **SIFT:** Our Python implementation of a baseline stitching solution inspired by current state-of-the-art feature-based microscopy stitching approaches, such as FRMIS (Mohammadi et al., 2024b). It uses SIFT (Lowe, 2004) features matched using Lowe's ratio test, RANSAC (Fischler and Bolles, 1981) for the estimation of translational and rotational tile transformation parameters, and Minimum Spanning Tree (MST) construction for global alignment. The MST is weighted by the number of feature matches and their estimated quality.
- **ORB:** Same as the **SIFT** baseline. Uses ORB (Rublee et al., 2011) features instead of SIFT.
- **MIST:** A state-of-the-art microscopy stitching method based on Normalised Cross-Correlation and MST construction (Chalfoun et al., 2017).
- **DEMIS-TR:** A modified version of DEMIS that estimates only translation parameters.

The following sections describe the results of our experiments.

6.1 Results on the EM424 Dataset

Since the EM424 dataset contains synthetically rotated images, we only evaluate the solutions that are capable of rotation estimation (i.e., SIFT, ORB, and DEMIS). The results, displayed in Table 1, show that both SIFT and DEMIS detect a high amount of feature matches, with DEMIS achieving the lowest reprojection error. This suggests a greater overall robustness of DEMIS compared to other methods. ORB, while being significantly faster than both SIFT and DEMIS, found a relatively low number of matches and reported the highest reprojection error. Despite that, ORB demonstrated similar stitching performance to SIFT, as evidenced by the almost identical values of RMSE, PSNR, SSIM and OFSIQA. We attribute this result to the use of RANSAC, which has the ability to filter out inaccurate matches. In this way, RANSAC helps to eliminate the influence that the higher reprojection errors have on the final output. DEMIS achieves the best stitching quality based on all metrics, although the improvements are marginal. We also highlight the similar behaviour of OFSIQA to RMSE, PSNR and SSIM, indicating its reliability as an image quality assessment metric.

6.2 Results on the Real-2x2 Dataset

The results on the Real-2x2 dataset are presented in Table 2. The dataset proved to be more challenging than EM424. This is evidenced by the much higher values of OFSIQA and by the decrease of mean match count. Despite that, DEMIS achieved considerably better stitching accuracy than other methods, with a 31% decrease in OFSIQA compared to ORB, the best performing traditional method, and a significant 1408% decrease in OFSIQA compared to MIST, a current state-of-the-art microscopy stitching solution. Additionally, DEMIS managed to retain the 1000 average matches (the maximum limit), which further demonstrates its robustness regardless of input data complexity. This is a common trait of learning-based approaches. Furthermore, while requiring a GPU, DEMIS achieves similar speed compared to other methods. Finally, the results suggest that translation might not be sufficient for precise microscopy image stitching. In particular, the translation-only DEMIS-TR reports a 12% higher value of OFSIQA than standard DEMIS. Figure 8 highlights the differences in the output of the evaluated methods.

In summary, the results demonstrate that DEMIS

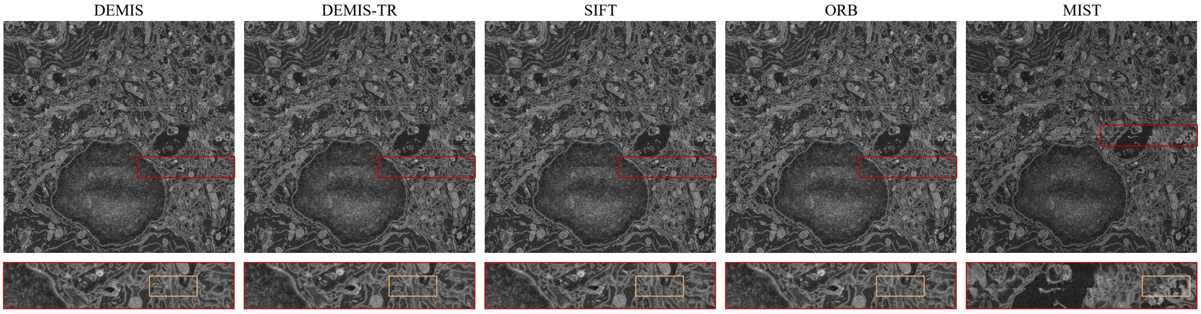

Figure 8: Comparison of the evaluated methods on an image from the Real-2x2 dataset. The seam between two stitched tiles is highlighted in red. Note that the seam of MIST (Chalfoun et al., 2017) is at a different position since MIST failed to stitch the image accurately. SIFT and ORB perform similarly and better than MIST. However, they produce significantly larger misalignments than DEMIS. DEMIS outputs the best result, which is slightly less misaligned than the result of DEMIS-TR.

Table 2: Stitching results on the Real-2x2 dataset. DEMIS, while being slower, achieves the best stitching quality by a large margin, especially compared to the intensity-based MIST. Estimating rotational parameters further improves the results. T and R correspond to translation and rotation estimation, respectively.

	Type	Seconds	Matches	OFSIQA
SIFT	T & R	0.39 (CPU)	923	3.00
ORB	T & R	**0.18 (CPU)**	94	2.98
MIST	T only	0.45 (CPU)	–	32.11
DEMIS-TR	T only	0.29 (GPU)	**1000**	2.56
DEMIS	T & R	0.29 (GPU)	**1000**	**2.28**

has higher stitching accuracy and robustness compared to approaches based on traditional methods. This is especially apparent as the complexity of the processed dataset increases. However, the increase in performance comes at the cost of requiring a system equipped with a GPU. Nevertheless, provided a system with a capable GPU is available, the speed of DEMIS is comparable to other methods.

7 CONCLUSIONS

We propose DEMIS, a novel method for stitching electron microscopy images based on LoFTR feature matching and global least squares optimisation at the level of individual features. Furthermore, we introduce EM424, a synthetic dataset generated by splitting existing high-resolution electron microscopy images into grids of overlapping image tiles. We evaluate DEMIS on the EM424 dataset and real-world data primarily using OFSIQA, a novel stitching quality metric based on optical flow. DEMIS performs significantly better than current microscopy stitching solutions, especially on real-world data. In particular, it reduces the value of OFSIQA reported by MIST from 32.11 to 2.28 (a 1408% improvement). We also demonstrate that estimating rotational parameters alongside translational parameters can further enhance stitching quality. Future work could investigate deep learning approaches other than LoFTR and the effects of estimating more complex transformations, such as affine or radially distorted transformations. Moreover, it could validate performance at different amounts of tile overlap. A decrease in the necessary overlap size could promote faster imaging.

ACKNOWLEDGEMENTS

We thank the company TESCAN 3DIM, our industrial partner, for providing valuable data for the Real-2x2 dataset.

REFERENCES

Alcantarilla, P. F., Bartoli, A., and Davison, A. J. (2012). Kaze features. In Fitzgibbon, A., Lazebnik, S., Perona, P., Sato, Y., and Schmid, C., editors, *Computer Vision – ECCV 2012*, Lecture Notes in Computer Science, pages 214–227, Berlin, Germany. Springer-Verlag.

Bay, H., Tuytelaars, T., and Gool, L. V. (2006). Surf: Speeded up robust features. In Leonardis, A., Bischof, H., and Pinz, A., editors, *Computer Vision – ECCV 2006*, Lecture Notes in Computer Science, pages 404–417, Berlin, Germany. Springer-Verlag.

Beyer, E., Sosinsky, G., Crum, J., Berthoud, V., Lichtensetin, A., and Geietta, G. (2009). The cell image library: Homo sapiens, multi-lamellar structure, hela. Dataset. CCDB:6348.

Bushong, E. and Deerinck, T. (2017). The cell image library: Mus, neuropil. Dataset. CCDB:8192.

Cardona, A., Saalfeld, S., Schindelin, J., Arganda-Carreras, I., Preibisch, S., Longair, M., Tomancak, P., Hartenstein, V., and Douglas, R. J. (2012). Trakem2 software for neural circuit reconstruction. *PLOS ONE*, 7(6):e38011.

Chalfoun, J., Majurski, M., Blattner, T., Bhadriraju, K., Keyrouz, W., Bajcsy, P., and Brady, M. (2017). Mist: Accurate and scalable microscopy image stitching tool with stage modeling and error minimization. *Scientific Reports*, 7:4988.

Chen, H., Luo, Z., Zhou, L., Tian, Y., Zhen, M., Fang, T., McKinnon, D., Tsin, Y., and Quan, L. (2022). Aspanformer: Detector-free image matching with adaptive span transformer. In Avidan, S., Brostow, G., Cissé, M., Giovanni, M., and Hassner, T., editors, *Computer Vision – ECCV 2022*, Lecture Notes in Computer Science, pages 20–36, Cham, Switzerland. Springer.

Conrad, R. and Narayan, K. (2021). Cem500k, a large-scale heterogeneous unlabeled cellular electron microscopy image dataset for deep learning. *eLife*, 10:e65894.

DeTone, D., Malisiewicz, T., and Rabinovich, A. (2018). Superpoint: Self-supervised interest point detection and description. In *Conference on Computer Vision and Pattern Recognition Workshops*, CVPRW, pages 337–349, Salt Lake City, UT, USA. IEEE.

Dice, L. R. (1945). A threshold selection method from gray-level histograms. *Ecology*, 26(3):297–302.

Ellisman, M., Ranganathan, R., Deerinck, T. J., Young, S. J., Hessler, D., and Terry, R. D. (1987). The cell image library: Homo sapiens, neocortex pyramidal cell. Dataset. CCDB:6355.

Fischler, M. A. and Bolles, R. C. (1981). Random sample consensus: A paradigm for model fitting with applications to image analysis and automated cartography. *Communications of the ACM*, 24(6):381–395.

Hoshijima, M., Hayashi, T., Thor, A., Terada, M., Martone, M., and Ellisman, M. (2004). The cell image library: Mus musculus, t-tubules, sarcoplasmic reticulum, myocyte. Dataset. CCDB:3603.

Huang, D., Chen, Y., Liu, Y., Liu, J., Xu, S., Wu, W., Ding, Y., Tang, F., and Wang, C. (2023). Adaptive assignment for geometry aware local feature matching. In *Conference on Computer Vision and Pattern Recognition*, CVPR, pages 5425–5434, Vancouver, Canada. IEEE.

Ilg, E., Mayer, N., Saikia, T., Keuper, M., Dosovitskiy, A., and Brox, T. (2017). Flownet 2.0: Evolution of optical flow estimation with deep networks. In *Conference on Computer Vision and Pattern Recognition*, CVPR, pages 1647–1655, Honolulu, HI, USA. IEEE.

Jolliffe, I. T. (2002). *Principal Component Analysis*. Springer New York, New York, NY, USA, 2 edition.

Kuglin, C. and Hines, D. A. (1975). The phase correlation image alignment method. In *Proceedings of the 1975 IEEE International Conference on Cybernetics and Society*, pages 163–165, New York, NY, USA. IEEE.

Lewis, J. P. (1995). Fast template matching. In *Vision Interface*, pages 120–123, Quebec City, Canada. Canadian Image Processing and Pattern Recognition Society.

Lewis, R. M., Baskaran, H., Green, J., Tashev, S., Paleologou, E., Lofthouse, E. M., Cleal, J. K., Page, A., Chatelet, D. S., Goggin, P., and Sengers, B. G. (2022). EMPIAR: Sbf sem of human term placental villi. Dataset. EMPIAR-10967.

Li, K. and Ding, G. (2018). A novel automatic image stitching algorithm for ceramic microscopic images. In *International Conference on Audio, Language and Image Processing*, ICALIP, pages 17–21, Shanghai, China. IEEE.

Liang, W. G., Wijaya, J., Wei, H., Noble, A. J., Mancl, J. M., Mo, S., Lee, D., King, J. L., Pan, M., Liu, C., Koehler, C. M., Zhao, M., Potter, C. S., Carragher, B., Li, S., and Tang, W. J. (2022). EMPIAR: Structural basis for the mechanisms of human presequence protease conformational switch and substrate recognition. Dataset. EMPIAR-10937.

Lowe, D. G. (2004). Distinctive image features from scale-invariant keypoints. *International Journal of Computer Vision*, 60(2):91–110.

Mahalingam, G., Torres, R., Kapner, D., Trautman, E. T., Fliss, T., Seshamani, S., Perlman, E., Young, R., Kinn, S., Buchanan, J., Takeno, M. M., Yin, W., Bumbarger, D. J., Gwinn, R. P., Nyhus, J., Lein, E., Smith, S. J., Reid, R. C., Khairy, K. A., Saalfeld, S., Collman, F., and da Costa, N. M. (2022). A scalable and modular automated pipeline for stitching of large electron microscopy datasets. *eLife*, 11:e76534.

Marquardt, D. W. (1963). An algorithm for least-squares estimation of nonlinear parameters. *Journal of the Society for Industrial and Applied Mathematics*, 11(2):431–441.

Mohammadi, F. S., Mohammadi, S. E., Adi, P. M., Mirkarimi, S. M. A., and Shabani, H. (2024a). A comparative analysis of pairwise image stitching techniques for microscopy images. *Scientific Reports*, 14:9215.

Mohammadi, F. S., Shabani, H., and Zarei, M. (2024b). Fast and robust feature-based stitching algorithm for microscopic images. *Scientific Reports*, 14:13304.

Muhlich, J. L., Chen, Y.-A., Yapp, C., Russell, D., Santagata, S., and Sorger, P. K. (2022). Stitching and registering highly multiplexed whole-slide images of tissues and tumors using ashlar. *Bioinformatics*, 38:4613–4621.

Otsu, N. (1979). A threshold selection method from gray-level histograms. *IEEE Transactions on Systems, Man, and Cybernetics*, 9(1):62–66.

Pizer, S. M., Amburn, E. P., Austin, J. D., Cromartie, R., Geselowitz, A., Greer, T., ter Haar Romeny, B., Zimmerman, J. B., and Zuiderveld, K. (1987). Adaptive histogram equalization and its variations. *Computer Vision, Graphics, and Image Processing*, 39(3):355–368.

Rublee, E., Rabaud, V., Konolige, K., and Bradski, G. (2011). Orb: An efficient alternative to sift or surf. In *International Conference on Computer Vision*, ICCV, pages 2564–2571, Barcelona, Spain. IEEE.

Sarlin, P.-E., DeTone, D., Malisiewicz, T., and Rabinovich, A. (2020). Superglue: Learning feature matching with graph neural networks. In *Conference on Computer Vision and Pattern Recognition*, CVPR, pages 4937–4946, Seattle, WA, USA. IEEE.

Schneider, C. A., Rasband, W. S., and Eliceiri, K. W. (2012). Nih image to imagej: 25 years of image analysis. *Nature Methods*, 9:671–675.

Shi, J., Ge, H., Wang, S., Wei, D., Yang, J., Cheng, A., Schalek, R., Guo, J., Lichtman, J., Wang, L., and Zhang, R. (2024). Two-stage error detection to improve electron microscopy image mosaicking. *Computers in Biology and Medicine*, 178:108456.

Sun, J., Shen, Z., Wang, Y., Bao, H., and Zhou, X. (2021). Loftr: Detector-free local feature matching with transformers. In *Conference on Computer Vision and Pattern Recognition*, CVPR, pages 8918–8927, Nashville, TN, USA. IEEE.

Teed, Z. and Deng, J. (2020). Raft: Recurrent all-pairs field transforms for optical flow. In Vedaldi, A., Bischof, H., Brox, T., and Frahm, J.-M., editors, *Computer Vision – ECCV 2020*, Lecture Notes in Computer Science, pages 402–419, Cham, Switzerland. Springer.

The MICrONS Consortium, Bae, J. A., Baptiste, M., Bishop, C. A., Bodor, A. L., Brittain, D., Buchanan, J., Bumbarger, D. J., Castro, M. A., Celii, B., Cobos, E., Collman, F., da Costa, N. M., Dorkenwald, S., Elabbady, L., Fahey, P. G., Fliss, T., Froudarakis, E., Gager, J., . . . , and Zhang, C. (2021). Functional connectomics spanning multiple areas of mouse visual cortex. Preprint.

Wang, Q., Zhang, J., Yang, K., Peng, K., and Stiefelhagen, R. (2023). Matchformer: Interleaving attention in transformers for feature matching. In Wang, L., Gall, J., Chin, T.-J., Sato, I., and Chellappa, R., editors, *Computer Vision – ACCV 2022*, Lecture Notes in Computer Science, pages 256–273, Cham, Switzerland. Springer.

Zhao, B., Zhang, K., Liu, P., and Chen, Y. (2023). Large-scale time-lapse scanning electron microscopy image mosaic using a smooth stitching strategy. *Microscopy Research and Technique*, 86(8):929–942.

Zhou, W., Bovik, A. C., Sheikh, H. R., and Simoncelli, E. P. (2004). Image quality assessment: from error visibility to structural similarity. *IEEE Transactions on Image Processing*, 14(4):600–612.